The International Journal of Advanced Manufacturing Technology (2019) 100:3127–3138
https://doi.org/10.1007/s00170-018-2855-3

ORIGINAL ARTICLE

Observation and analyzation of plasma channel evolution behavior in air flushing electrical arc machining

Yingmou Zhu[1] · Lin Gu[1] · Ahmad Farhadi[1] · Guojian He[1] · Wansheng Zhao[1]

Received: 4 July 2018 / Accepted: 3 October 2018 / Published online: 26 October 2018

Abstract
Blasting erosion arc machining (BEAM) is a novel and promising electrical machining process for difficult-to-cut material processing. In this research, air is applied as an alternative dielectric to investigate the feasibility of dry BEAM. An arc plasma observation experiment is designed and conducted based on a four-channel intensified charge-coupled device (ICCD) high-speed camera in order to observe and investigate the arc plasma expansion and deflection behavior. Furthermore, the influence of the aerodynamic force on plasma column deflection is also studied through comparing the images under different airflow velocities. Voltage and current waveforms were captured to verify the positive effect of air flushing on plasma channels' deflection behavior. Additionally, crater geometries on the workpiece and electrodes were also observed and discussed as a means to analyze the effect of airflow on machining characteristics. The experimental results reflected that aerodynamic arc disturbing mechanism can be realized in air flushing BEAM, which is a promising process of working fluid for BEAM.

Keywords Blasting erosion arc machining (BEAM) · Air dielectric · Arc plasma channel expansion · Plasma movement · Crater geometry

1 Introduction

Blasting erosion arc machining (BEAM) is widely applied for machining difficult-to-cut materials due to its low cost and excellent material removal capability. Recently, Xu [1], Chen [2], and Gu [3] investigated the machining characteristics of blasting erosion arc machining processes of Inconel 718 alloy, Ti-6Al-4V, and SiC/Al metal matrix composites, separately. Their research results reflected that compared to other conventional methods, this process was able to achieve a higher material remove rate (MRR) by applying high-energy density electrical arc accompanied with limited tool wear ratio (TWR). During BEAM machining, because a stationary arc will damage the workpiece surface and should be avoided, hydrodynamic arc breaking mechanism (HABM) [4] was induced by applying high-velocity dielectric flushing. Under this scenario, the arc is elongated or even broken by the hydrodynamic force. In order to further disclose the mechanism of HABM, Gu et al. [5] observed the development of the plasma channel and also analyzed the machining characteristics of a single arc discharge. After, Zhang et al. [6] studied the high-velocity flushing effect in BEAM machining through applying the computational fluid dynamic (CFD) method. Their results indicate that high-velocity water flushing can not only break off the stable and continuous arcing, but can also form a low-pressure area on the downstream side of the electrode, which could expel the melting metal into the surrounding dielectric—greatly improving the material removal rate. Up to now, various BEAM research experiments mainly focus on machining in water-based dielectric. When considering the demands of simplification of the equipment and environmental friendliness, using pressured air rather than conventional water-based dielectric is a variable option. However, whether the pressured air can achieve a similar arc breaking effect as water-based dielectric is still unknown and requires further study.

✉ Lin Gu
lgu@sjtu.edu.cn

[1] State Key Laboratory of Mechanical System and Vibration, School of Mechanical Engineering, Shanghai Jiao Tong University, Shanghai, China

Until now, researchers have studied the machining performance of electrical discharge machining (EDM) along with other electrical arc machining (EAM) in air dielectric. Kunieda et al. [7] initially proposed electrical discharge machining in gas, known as dry EDM. This novel process was characterized by significantly low tool wear ratio, a thinner white layer, and a narrower discharge gap [8, 9]. However , their research mainly focused on the EDM rather than the EAM field. In order to distinguish EDM and EAM, Zhang et al. [10] researched the plasma tunnel and crater geometry on a single pulse discharge, and their results obtained a discriminatory line between EDM and EAM. Later, Shen et al. [11] proposed an EAM method in air dielectric known as high-speed dry compound electrical machining. Their research indicates that compared to conventional EDM, dry EAM can also achieve relatively high MRR. However, how the air flushing affects the discharge arcing is not further studied. The majority of research mainly focused on the parameter optimization, but the formation and deflection of the arc plasma channel as well as the crater formation were not studied yet.

In order to better understand the mechanism of air flushing BEAM process, the arc plasma channel expansion and arc movement behavior were observed and studied in this research. Firstly, the arc plasma developing process and arc column self-magnetic compression effect were analyzed. Then, the mechanism of the arc plasma channel expansion and deflection behavior were captured and studied with a high-speed camera. Additionally, the plasma column movement was also researched by comparing the images under different air flushing velocities. Discharge waveforms of voltage and current were collected and studied to investigate and identify the influence of air flushing on plasma channel. In addition, the crater morphology on workpiece and electrode was analyzed to disclose the effect of air flushing on machining characteristic of air flushing BEAM.

2 Influence of horizontal airflow on plasma arc column

Arc plasma is a kind of ionized gaseous substance, which is ignited by the spark discharge between the two electrodes and develops quickly into arc column with the increasing discharge current [12]. Moreover, Kojima A et al.[13] found that the plasma in a long-pulse duration EDM process was in thermal equilibrium due to the temperatures of different atom species in plasma were equal. Therefore, the plasma in arc discharging can also be treated as under a local thermodynamic equilibrium (LTE) state because it has a much longer pulse duration (usually longer than 1 ms). Because the electrodes are needle and plate shape in single arc discharging, the arc plasma is cone-shaped when it is stable without flushing [14, 15]. During arc discharging under air flushing condition, the horizontal airflow will induce the plasma arc column movement due to air flushing generating the horizontal aerodynamic force. However, as well-known, the plasma arc column also exists the self-magnetic compression effect since the variable current generates the Lorentz forces in the magnetic field. The self-magnetic compression of plasma column also generates an additional pressure, which will impede the plasma arc column movement when the horizontal airflow affects the arc plasma column. In order to further investigate the phenomenon, the simplified self-magnetic compression model in static air dielectric was analyzed firstly. Then, the influence of airflow on plasma arc column and definition of arc plasma movement were introduced in this section. Based on those basic theories, the following observation experiment can better analyze the mechanism of arc plasma expansion and movement.

2.1 Analysis of arc column self-magnetic compression

Figure 1 shows the schematic view of self-magnetic compression. Considering a point in plasma column, the equilibrium equation of volume force can be given as following:

$$\frac{dP}{dr} + j_z B_\phi = 0 \tag{1}$$

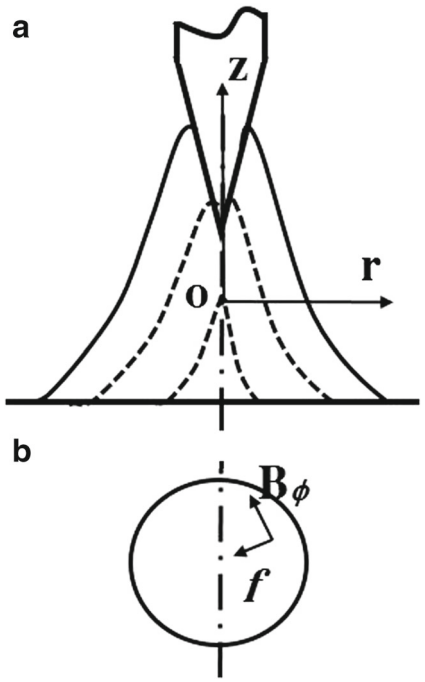

Fig. 1 The schematic view of self-magnetic compression: **a** profile section, **b** cross section

Where P is the pressure, j_z is the axial current density, and B_ϕ is the intensity of self-magnetic field. The physical explanation of this equilibrium equation is that the Lorenz force of plasma arc column will be balanced by the pressure gradient of the plasma channel.

Among the plasma arc column, the intensity of magnetic field can be deduced based on ampere circuit law. Due to the symmetry of arc column, the intensity of magnetic field is given as:

$$B_\phi = \frac{\mu}{r}\int_0^r j_z r dr \tag{2}$$

Where μ is the magnetic permeability of dielectric and j_z is the axial current density. When substituting Eq. 2 into Eq. 1, the pressure of arc column can be deduced as:

$$dP = -\mu\left(\frac{j_z}{r}\int_0^r j_z r dr\right)dr \tag{3}$$

The axial current density in the arc column is assumed to accord with a parabola distribution, then the j_z can be given as (r_* is the radius of current channel in arc column):

$$j_z = \frac{I}{\pi r_*^2}\left(1 - \frac{r^2}{r_*^2}\right) \tag{4}$$

When integrating the pressure from the edge of arc column to its center position, the pressure of arc column can be given as:

$$P(r) = \frac{5}{3}\frac{\mu}{4\pi}\frac{I^2}{\pi r_*^2}\left(1 - \frac{12}{5}\frac{r^2}{r_*^2} + \frac{9}{5}\frac{r^4}{r_*^4} - \frac{2}{5}\frac{r^6}{r_*^6}\right) + P_0 \tag{5}$$

Where I is the current of arc plasma column, r_* is the radius of current channel in arc column and P_0 is the ambient pressure at the edge of the arc column.

Defining the $\Delta P(r)$ as additional increment in pressure generated by the self-magnetic compression, which can be represented as $\Delta P(r) = P(r) - P_0$. Therefore, the additional increment in pressure value at radius position of r can be deduced as following:

$$\Delta P(r) = \frac{5}{3}\frac{\mu}{4\pi}\frac{I^2}{\pi r_*^2}\left(1 - \frac{12}{5}\frac{r^2}{r_*^2} + \frac{9}{5}\frac{r^4}{r_*^4} - \frac{2}{5}\frac{r^6}{r_*^6}\right) \tag{6}$$

As analyzed in Eq. 6, the additional increment in pressure value is related to the radius position, r, and the current channel radius of arc column, r_* . The $\Delta P(r)$ increases as the current increases, but decreases as the current channel radius of arc column increases. While, the current channel radius of arc column is determined by the plasma channel radius, which changes along with the z position as shown in Fig. 1. Therefore, the additional increment in pressure value is variable at different positions in plasma arc column, resulting in the interaction of additional increment in pressure and air flushing effect is also different.

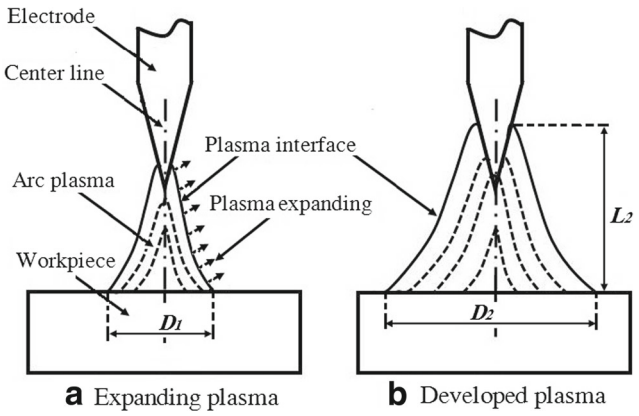

Fig. 2 Schematic arc plasma developing under no air flushing condition

2.2 Arc plasma expansion and deflection

When the air flows through the arc plasma column, there exists a pressure difference between the plasma front interface and plasma back interface. The pressure difference can induce the arc plasma column moving along with the air flushing direction. In order to study how the horizontal air flushing affects the arc plasma, the types of plasma channel expanding and developing are defined firstly. According to the previous experimental results [15], the schematic diagram of the arc plasma developing under no air flushing condition can be reflected in Fig. 2. After the arc plasma ignited, the plasma interface expands due to the ionization of the surrounding air dielectric. In the expansion stage, the speed of diameter enlargement can be regarded as the arc plasma expansion speed, v_e. In Fig. 2b, when the input heat source of arc plasma and the dissipative heat of arc plasma reach the equilibrium mode, the plasma interface remains stable and the diameter remains almost invariable.

As depicted in Fig. 2, defining the diameter of expanding plasma as D_1 and the diameter of developed plasma as D_2, the average expansion speed of arc plasma in this stage can be reflected as:

$$v_e = \frac{D_2 - D_1}{t} \tag{7}$$

After the arc plasma is ignited and extended, it reaches the mature stage and the LTE mode. Since the arc plasma is tender and slender, the arc plasma state will be affected by the airflow when flushing exists in the gap. In order to better study how the airflow affects the arc plasma, it is necessary to define the motion behavior of the arc plasma under air flushing conditions. Figure 3 shows the schematic diagram of arc plasma moving under air flushing conditions. In order to define the arc plasma movement, the position of the arc plasma is represented by the center line of arc

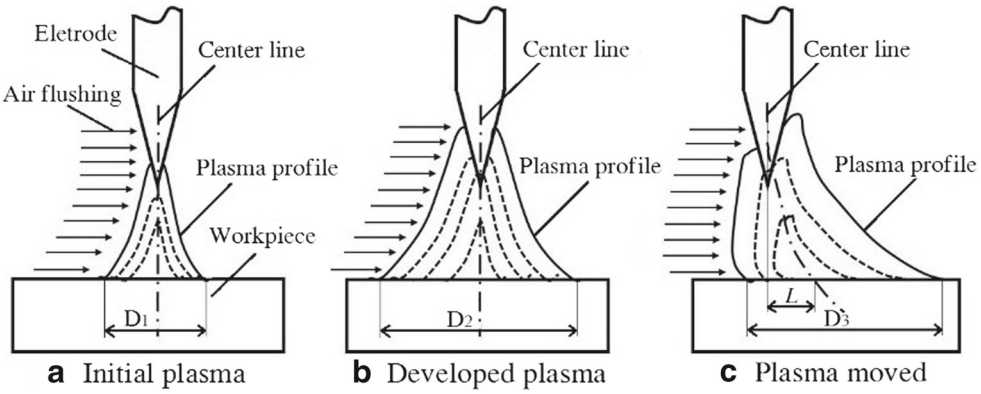

Fig. 3 The schematic diagram of arc plasma movement

column. Therefore, the motion of arc plasma is represented by the movement of the center line, as shown in Fig 3.

As can be observed in Fig. 3, the formed initial plasma is a symmetrical cone shape, which means it is almost insensitive to the airflow (the reason why the formed initial plasma is almost insensitive to airflow will be explained in the following sections). However, as the arc plasma develops, the plasma distorts due to the influence of aerodynamic force. The plasma front interface which faces the flushing direction will be compressed and the back interface of arc plasma will be extended conversely. As a result, the arc plasma shape distorts and its center line also curves along the air flushing. Therefore, the center line movement is defined as the speed of arc plasma movement, v_m. As indicated in Fig. 3, through defining the movement distance of the arc plasma center line as L and the used time

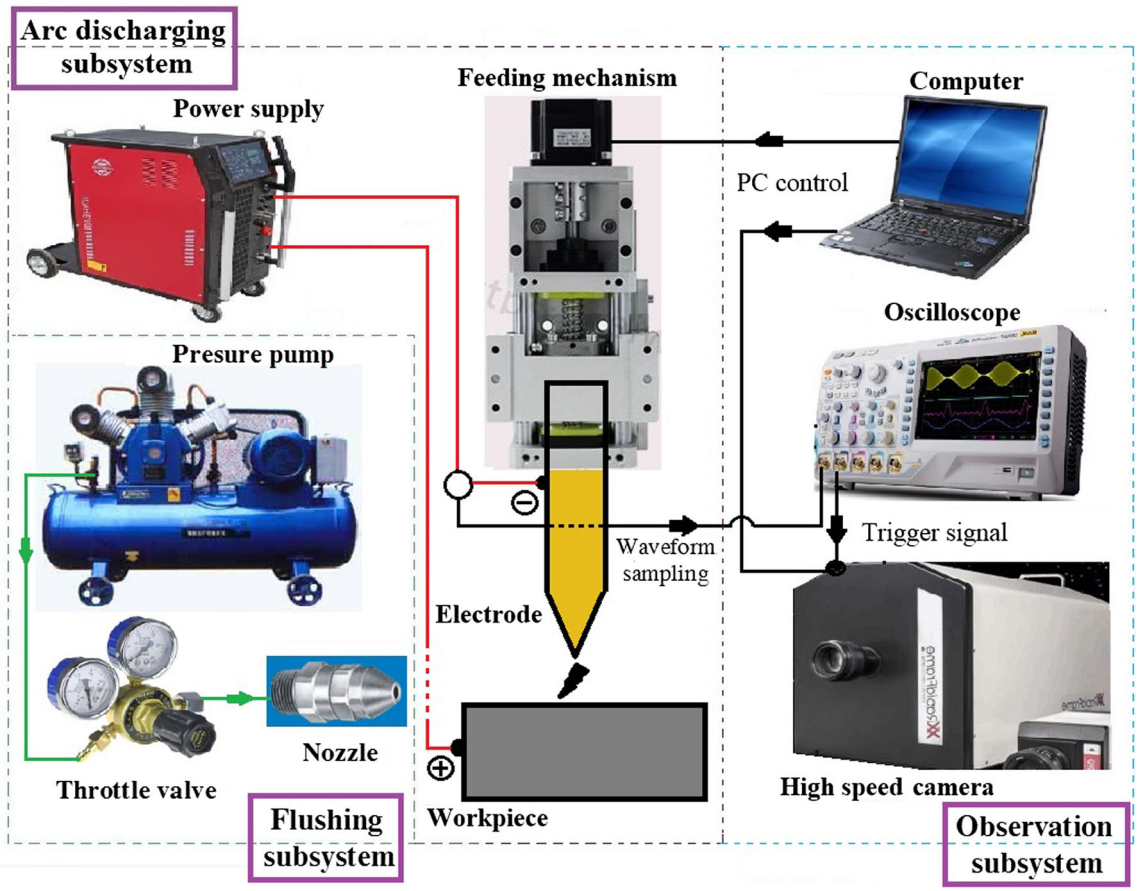

Fig. 4 Scheme of single arc discharge system

as t, the average movement speed of arc plasma during this period can be given as:

$$v_m = \frac{L}{t} \tag{8}$$

3 Arc plasma observation methodology and experimental design

The above definition of arc plasma development and movement in airflow only describes the tendency of plasma evolution. Moreover, the basic theoretical analysis indicates that the self-magnetic compression will affect the arc plasma movement. In order to further understand the mechanism of arc plasma evolution in air flushing condition, an observation experiment is designed and conducted.

3.1 Experimental setup

It is difficult to observe the arc plasma evolution in a continuous discharge because both working liquid splashing and debris expelling influence the observation effect. Because of this, the single discharge experiment is regarded as an effective and feasible method used to investigate the discharge phenomenon [16, 17].

As shown in Fig. 4, the observation experimental setup consists of flushing, discharging, and observing subsystems. In observing subsystem, a high-speed camera (type XXRapidFrame, made by Standford company) with four intensified charge-coupled devices (ICCDs) was applied to capture and record the arc plasma profile. Due to each ICCD can only record and save several images in each time, the name of frame rate was avoided in this paper. While, the minimum exposure time of each ICCD is 200 ps, and the interval time of each ICCD can be set independently. An AF Micro-Nikkor lens (type 60 mm f/2.8D) was attached to the camera for a great magnification of discharge as well as better clearance of photos. Moreover, an oscilloscope was utilized to trigger the camera and record the peak current as well as the gap voltage. In the discharging subsystems, a 2-mm-diameter cylinder copper with a sharp tip served as the needle electrode and a die steel plate serves as the plate workpiece. The gap between the electrode and workpiece was controlled by a feeding unit. A pulse generator was utilized as a means to supply the discharge energy. The flushing subsystem consists of an air compressor pump and pressure tank, a small nozzle as well as some control valves and pressure pipes. A 2-mm-diameter nozzle and 0.8-MPa tank pressure could help to realize high-speed air flushing, and the different airflow speeds were achieved by controlling the flow rate of control valves. The air flushing velocity was measured by a digital anemometer (type GM8909, range 0–45 m/s). Besides, in order to ensure a relatively horizontality of airflow, the nozzle outlet is parallel to the workpiece surface, and it also placed at the same height as the workpiece upper surface.

3.2 Arc plasma evolution observation experiment design

The aim of this experiment was to observe and study the formation, expansion, and excursion of plasma channel under high-velocity air flushing. In order to clearly observe the development of the plasma column, the discharge current was set to 500 A to achieve a large and bright arc plasma. The pulse duration was 5 ms and the air flushing velocity was 35 m/s. Additionally, the exposure time of each ICCD was 100 ns, and the interval of each image was set according to the user and experimental requirement. The time of voltage drop at ignition was regarded as 0. Due to the plasma size and shape which vary obviously in the beginning stage, the interval time of each image was set to a small amount at this stage.

3.3 Flushing velocity observation experiment design

The aim of this experiment is to investigate the influence of air flushing velocity on arc plasma movement. In order to disclose the influence of flushing velocity on the arc column distortion, the discharge parameters such as peak current and pulse duration were same as those of the previous experiment. Six typical time points were chosen to record the images of arc plasma column geometry, which were 100 μs, 200 μs, 400 μs, 1000 μs, 3000 μs, and 5000 μs, respectively. Other conditions are listed in Table 1. The crater geometry and electrode shape after discharge were analyzed utilizing a Zeiss Stemi 2000-C stereomicroscope.

4 Observation experiment results of arc plasma evolution

By means of the high-speed camera, the arc plasma column geometry in air flushing condition (flushing velocity 35 m/s) was obtained according to the preset time point,

Table 1 Parameters of observation experiment

Parameter	Values
Needle electrode	Copper (negative)
Open voltage [V]	90
Discharge current [A]	500
Pulse duration [ms]	5
Flushing velocity [m/s]	0, 15, 30, 45

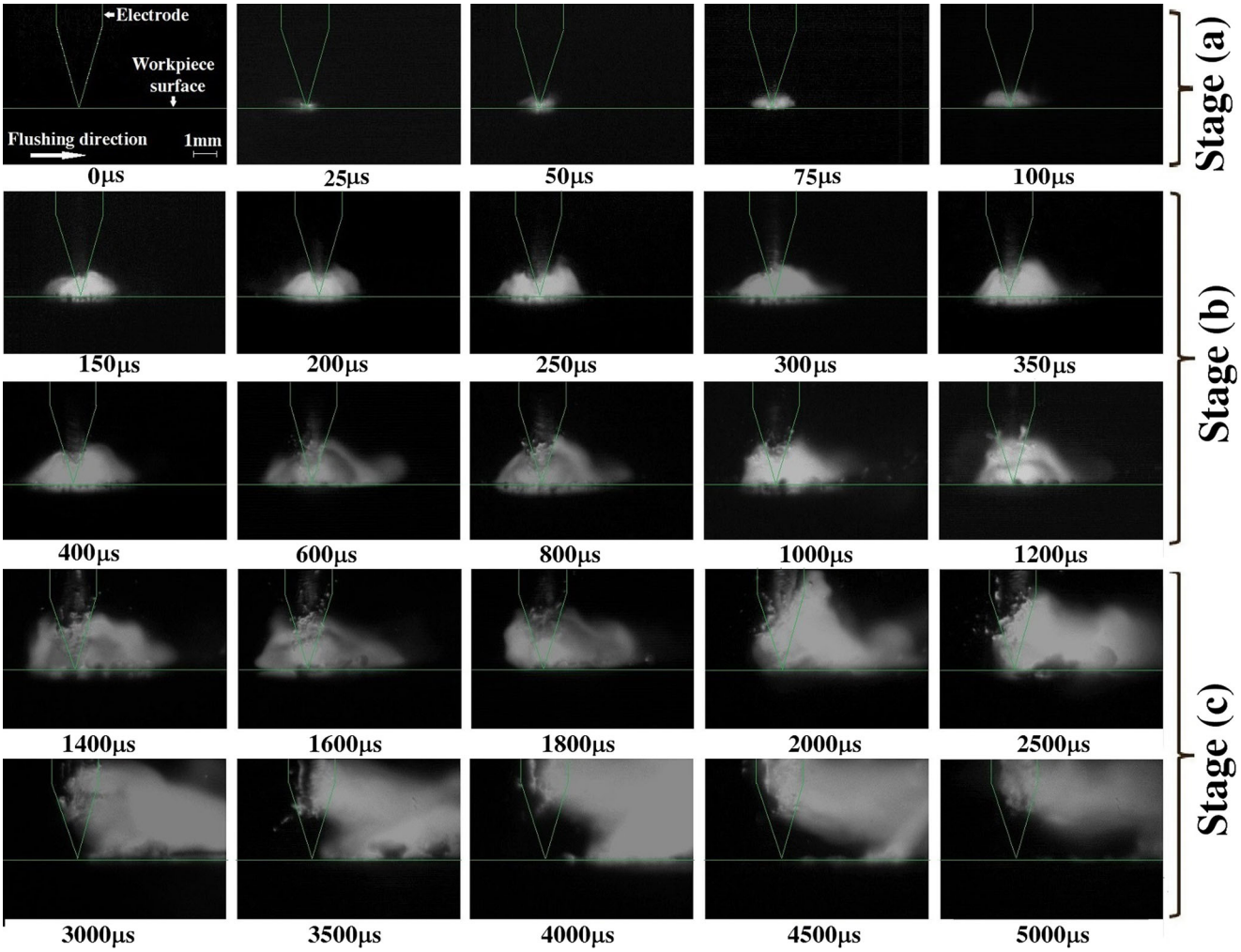

Fig. 5 Arc plasma column geometry in each record time: **a** ignition and rapid radial expansion stage, **b** full expansion stage, **c** distortion stage

as depicted in Fig. 5. The outline of the needle-plate electrode was marked in the images in order to recognize the behavior of arc plasma column. The images in Fig. 5 indicate that the arc plasma column experienced three stages during the entire pulse duration—rapid radial expansion, full expansion and deflection (or distortion). At 0 μs, the discharge was ignited and the image was completely dark since the discharging channel was not completely built.

4.1 Arc plasma expansion

By comparing the photographs in group (a) of Fig. 5, it is clear that the diameter of plasma column expands rapidly as discharge continues, while its length almost remained constant before the time of 100 μs. Consequently, this stage can be regarded as the ignition and rapid radial expansion stage. It is also notable that, compared to the subsequent images, the arc plasma column is almost insensitive to the air flushing at this stage and remained symmetric to the electrode centerline. At the time of 25 μs, the discharge plasma has already formed but the plasma channel was still weak since the discharge was in its initial stage and the current was relatively small (it takes about 250 μs for the current to increase to the setting value 500 A, as shown in Fig. 7). When the discharge lasted for 100 μs, the arc plasma expanded radially with the increase of the discharge current. The diameter and length of the arc plasma are about 2.2 mm and 0.8 mm, respectively. At that time, a clear initial arc plasma shape was formed, which was similar to the subsequent plasma geometry. Furthermore, when considering the average radial expansion speed of arc plasma, v_{re}, the arc plasma diameters under the times of 25 μs and 100 μs can be measured. The calculated average expansion speed can reach up to 20 $\mu m/\mu s$ (20m/s) in this rapid radial expansion stage.

During the full expansion stage, the diameter and length of the arc plasma developed as the discharge continued which is reflected in Fig. 5b. Throughout the beginning

of this stage (150 μs), the diameter and length of the arc plasma size were measured to be approximately 2.9 mm and 1.0 mm, respectively. After the arc plasma entirely expanded, its diameter and length can reach up to 5.0 mm and 2.0 mm correspondingly at 1200 μs. In this stage, the average radial expansion speed of arc plasma, v_{re}, was only about 1.8 $\mu m/\mu s$ (1.8 m/s), which is much slower than that in the radial expansion stage. Reasonable explanation is perhaps because in the previous stage, the increasing discharge current has the primary contribution to the rapid radial expansion of the arc plasma. While at the full-expansion stage, the plasma self-evolution dominates the arc plasma column development since the discharge current remains the same at this period.

Throughout the arc discharging, although the gap size is set as dozens of micron at first, it looks that the electrode tip was surrounded by the arc plasma column and the arc column length continuously increased in the full-expansion stage. This phenomenon was influenced by the needle electrode erosion and arc plasma development. As the electrode tip was eroded, the discharge gap would increase and the length of the plasma column increased correspondingly [15].

4.2 Plasma column projection

As shown in Fig 5c, it is clear that the arc plasma column was elongated and distorted significantly after 1400 μs of ignition. This phenomenon of arc plasma column distortion influenced by air flushing can be regarded as the result of aerodynamic arc disturbing mechanism (ACDM), a particular hydrodynamic arc breaking mechanism (HABM) which uses air rather than liquid as the working dielectric. Furthermore, the arc plasma remained stable at the beginning of discharging and only slid on the workpiece surface after it fully expanded. Furthermore, compare all the images throughout the arc discharging, the arc plasma expands at first, and then it moves along with air flushing direction after full development. As depicted in Fig 5c, the plasma column slid mildly in the previous 2000 μs. In this period, the front interface of the plasma was obviously compressed, and a long tail stretched along the air flushing direction at its back interface. Compared to the initial ignition position, the arc plasma offset distances were about 0.75 mm and 1.86 mm at the time of 1400 μs and 2000 μs, respectively. Therefore, the average moving velocity of the arc plasma vm was about 1.85 m/s during this period. After 2000 μs of ignition, the arc plasma column was noticeably stretched and the deviation of arc plasma was about 6.62 mm at the time of 3500 μs. This is not to mention that the arc plasma column was completely blown to the back of the electrode. The average movement velocity of arc plasma, v_m, was about 3.2m/s during this period.

4.3 Analysis of plasma column projection

As analyzed above, an important rule of arc plasma projection is that the arc plasma channel firstly expands and then slides. A reasonable explanation is that the resistant force formed by plasma column varies obviously in the radial and full expansion stages. In order to suppose the explanation above, the value of additional increments in pressure of plasma arc column at different stages is considered.

As shown in Eq. 6, since the additional pressure increment is the function of r, it is difficult and complex to consider the additional increment in pressure of all the positions in radius direction. Thus, the maximum additional increment in pressure , $\Delta P(r)_{max}$, is introduced to represent the resistant pressure in this research.

$$\Delta P(r)_{\max} = \Delta P\,(0) = \frac{5}{3}\frac{\mu}{4\pi}\frac{I^2}{\pi r_*^2} \tag{9}$$

Equation 9 indicated that the value of maximum additional increments in pressure is proportional to the square of the discharge current and inversely proportional to the radius of the current channel. According to the theory proposed by Steenbeck [18], the arc plasma channel consists of the conductive current channel and non-conductive channel. In general, the radius of current channel in arc column keeps the same variation tendency as the radius of arc plasma channel, but usually smaller than the radius of arc plasma channel, while it is difficult to obtain the radius of current channel in real arc discharging condition. Therefore, the radius of arc plasma channel can be applied to qualitatively distinguish the value of additional increment in pressure among different stages.

As shown in Fig. 5, compared to the arc plasma diameter in distortion stage, the arc plasma diameter is much smaller in rapid radial expansion stage and full expansion stage. Thus, the radius of current channel is also smaller in those two stages correspondingly. Therefore, the maximum additional increment in pressure is also large in those two stages correspondingly compare to that of distortion stage. As a result, the arc plasma channel does not slide along with air flushing in those two stages. After the arc plasma was fully expanded and the plasma column diameter has already reached a high value and the current density of the plasma channel dropped correspondingly. Therefore, the additional increment in pressure of the plasma column also decreased. As a result, the plasma was apt to be influenced by the hydrodynamic force in the second stage.

Additionally, the degree of plasma arc column deflection near workpiece side is more obvious if compared to that of plasma arc column deflection near the electrode. To investigate the reason of this phenomenon, the radius variation of the current channel radius at z axis is

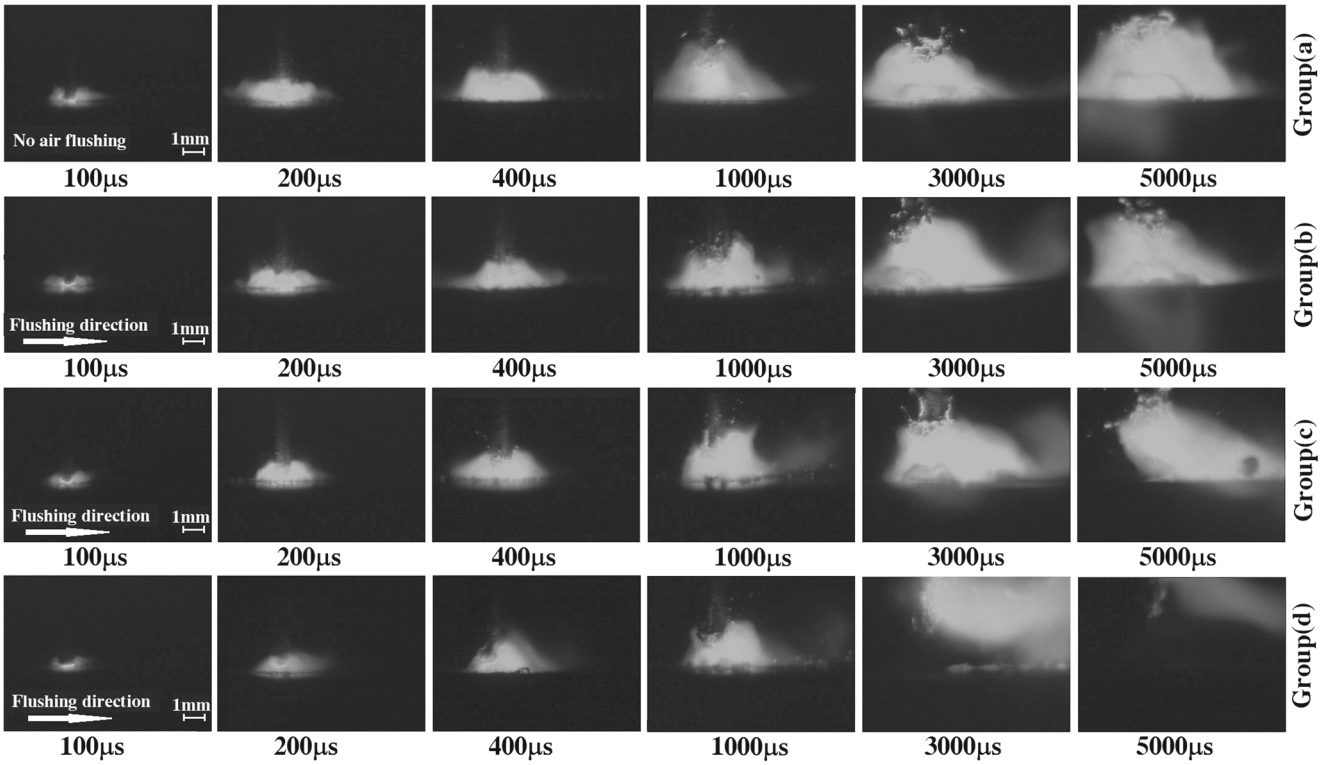

Fig. 6 Influence of air flushing velocity on plasma column: **a** no flushing, **b** 15 m/s, **c** 30 m/s, **d** 45 m/s

considered. Due to the cone shape of plasma arc column, the radius of plasma arc column is increased from the electrode side to the workpiece side, resulting in the radius of current channel in arc column is also different at different z positions. The radius of current channel near electrode side is smaller than that of radius near workpiece side. As a result, the maximum additional increment in pressure is larger near electrode side compared to that of value near workpiece side. Thus, the degree of plasma arc column deflection near workpiece side is more significant.

5 Influence of air flushing velocity on machining effect

This section focuses on analyzing the influence of air flushing velocity on plasma column movement through observing and analyzing the arc plasma shape, discharge waveform, workpiece crater geometry, and electrode erosion.

5.1 Influence of flushing velocity on arc plasma column shape

As shown in group (a) of Fig. 6, it is obvious that without flushing, the shape of the arc plasma column remained a symmetrical cone shape during discharging, which is similar to the plasma in arc welding [19, 20]. However, when air flushing existed, the arc plasma column would slide and distort from 1000 μs, as shown in groups (b)–(d) of Fig. 6. Furthermore, the distortion elongated as the air flushing velocity increased.

As can be observed in Fig. 6b, when the flushing velocity was relatively slow (15 m/s), the distortion of the arc plasma column was very limited, similar to that of without air flushing. However, when the flushing velocity increased to 30 m/s, even 45 m/s, the arc plasma was obviously compressed before 1000 μs, which is noticeably smaller than that of the no air flushing condition. A reasonable explanation was that the pressured air significantly impeded the plasma channel expansion process. Furthermore, the arc plasma column obviously moved and slid after 1000 μs under those conditions, and the beginning time of the arc plasma column excursion was earlier as the flushing velocity increased. Additionally, as Fig. 6d reflects, the arc plasma channel was almost broken off by the air flushing at the time of 5000 μs, which indicates that the 45 m/s air flushing velocity can achieve aerodynamic arc breaking mechanism.

In order to better explain the phenomena in Fig. 6, the discharge waveforms of voltage and current under different air flushing velocities are shown in Fig. 7. As can be observed from Fig. 7a and b, the discharge current remained steady after it reached the setting value, and the discharge voltage remained constant after the ignition. This waveform

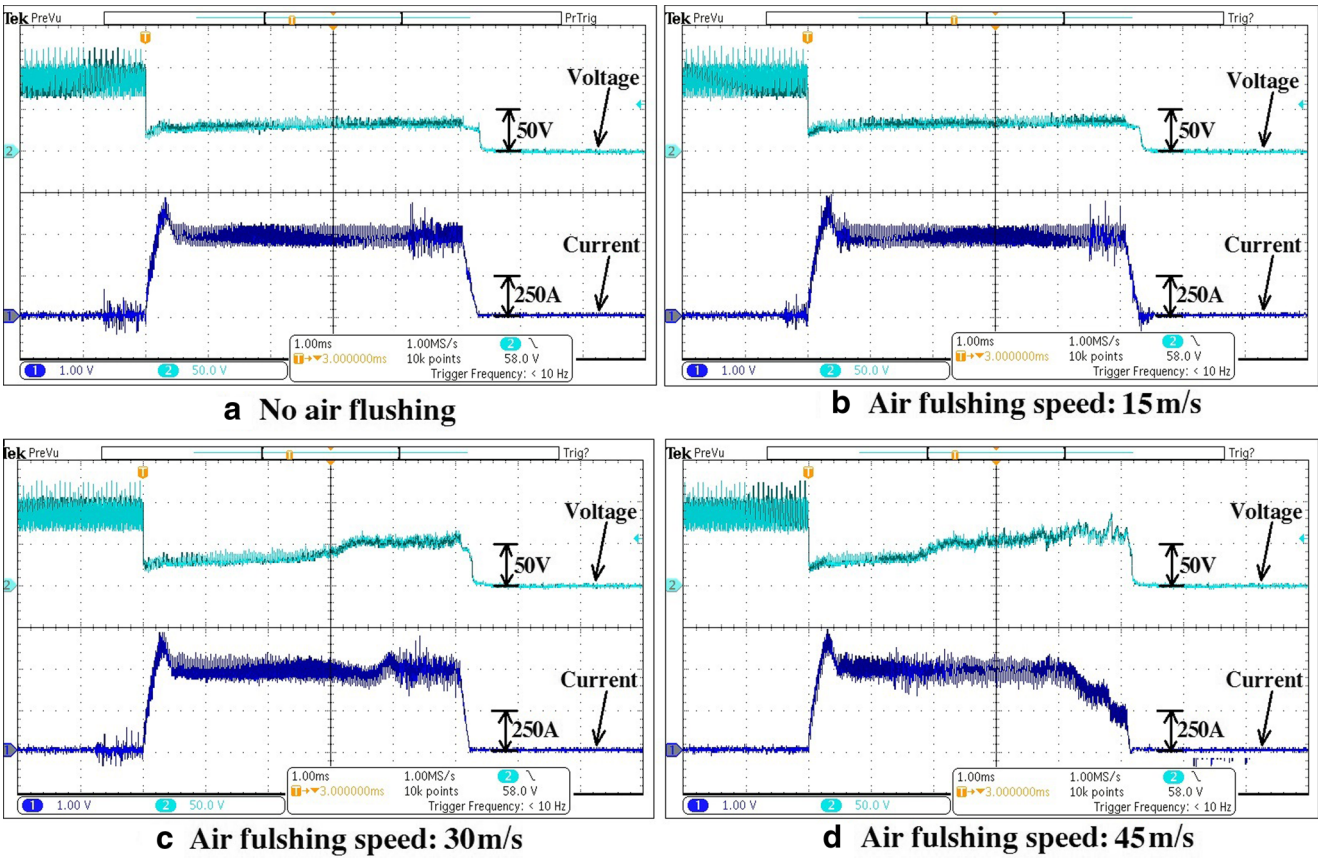

Fig. 7 Discharge waveforms of different air flushing velocity: **a** no flushing, **b** 15 m/s, **c** 30 m/s, **d** 45 m/s

indicates that arc plasma column is not disturbed obviously under those two velocities. This also can be supported by the images in groups (a) and (b) of Fig. 6. However, when the air flushing velocity increased to 30 m/s or even 45 m/s, the discharge waveforms underwent an obvious fluctuation, as shown in Fig. 7c and d. It is clear that the discharge voltage dropped to 30 V at first, then increased to 60 V subsequently. Correspondingly, the discharge current noticeably fluctuated. This phenomenon also reflects that the arc discharging states (including the arc plasma and discharge waveform) were affected obviously by the high-velocity air flushing.

When the air flushing velocity was 30 m/s, the gap voltage began to increase at the time of 3000 μs, which is synchronous with the current fluctuation, as shown in Fig. 7c. If the flushing velocity increased to 45 m/s, the current remained in most of this discharge duration, but decreased obviously at the end and the gap voltage increased significantly. It indicates that the plasma column was elongated to a near broken status by the hydrodynamic force, which also proves the feasibility of hydrodynamic arc breaking mechanism in air-based electrical arc machining.

5.2 Influence of flushing velocity on crater morphology

Figure 8 shows the craters generated on a plate workpiece surface under various air flushing velocities. The geometry of these craters was quite different from each other. Under the condition of without flushing, the crater geometry was circular and the recast molten metal built up at the peripheral of the crater. However, when the arc plasma was disturbed by flushing, the crater geometry varied and the recast molten metal around the crater was eliminated. Especially, when the air flushing velocity increased to 45 m/s, it formed a specific crater with a shallow long trail, as indicated in Fig. 8b.

The variation of crater geometries under the different flushing velocities reflects the influence of air flushing conditions on the material removal mechanism. Without air flushing, the arc plasma column remains stable at its original position throughout the entire discharge period and leads to a large crater, but the molten metal is prone to recast onto the peripheral of the crater and results in a thick recast layer. However, when effective air flushing is present, the arc plasma column is disturbed and results in a different

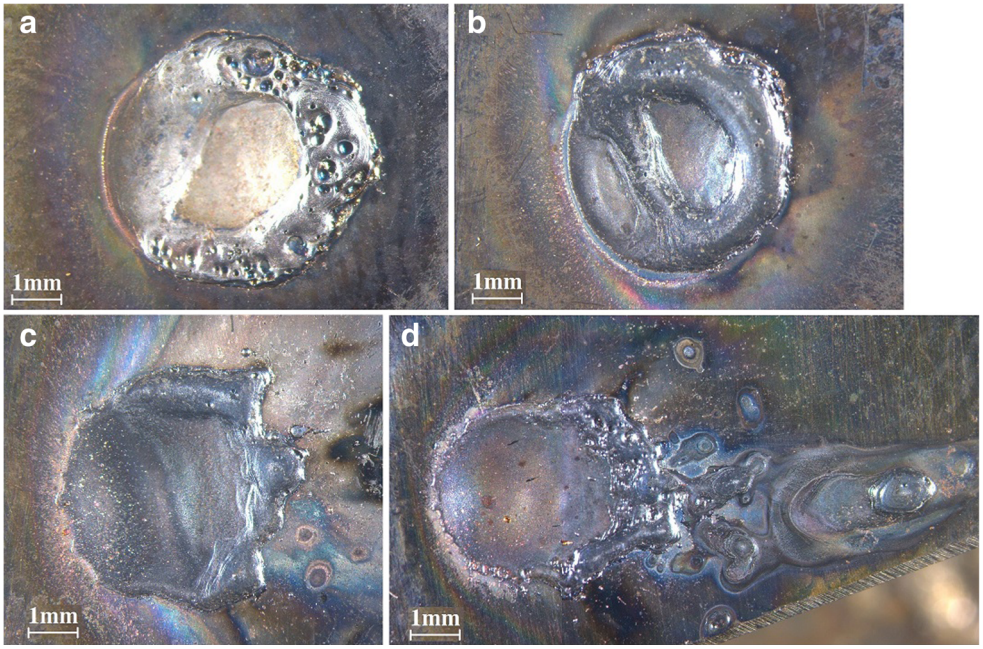

Fig. 8 Crater geometry of workpiece after single arc discharge: **a** no flushing, **b** 15 m/s, **c** 30 m/s, **d** 45 m/s

morphology crater, as shown in Fig. 8b–d. Additionally, the molten metal is more effectively expelled from the molten pool and seldom recasts near the crater, which indicates that air flushing can obviously improve the material removal efficiency.

5.3 Influence of flushing velocity on electrode erosion

Figure 9 depicts the shape of the eroded needle electrode under different flushing conditions. The electrode tip shape

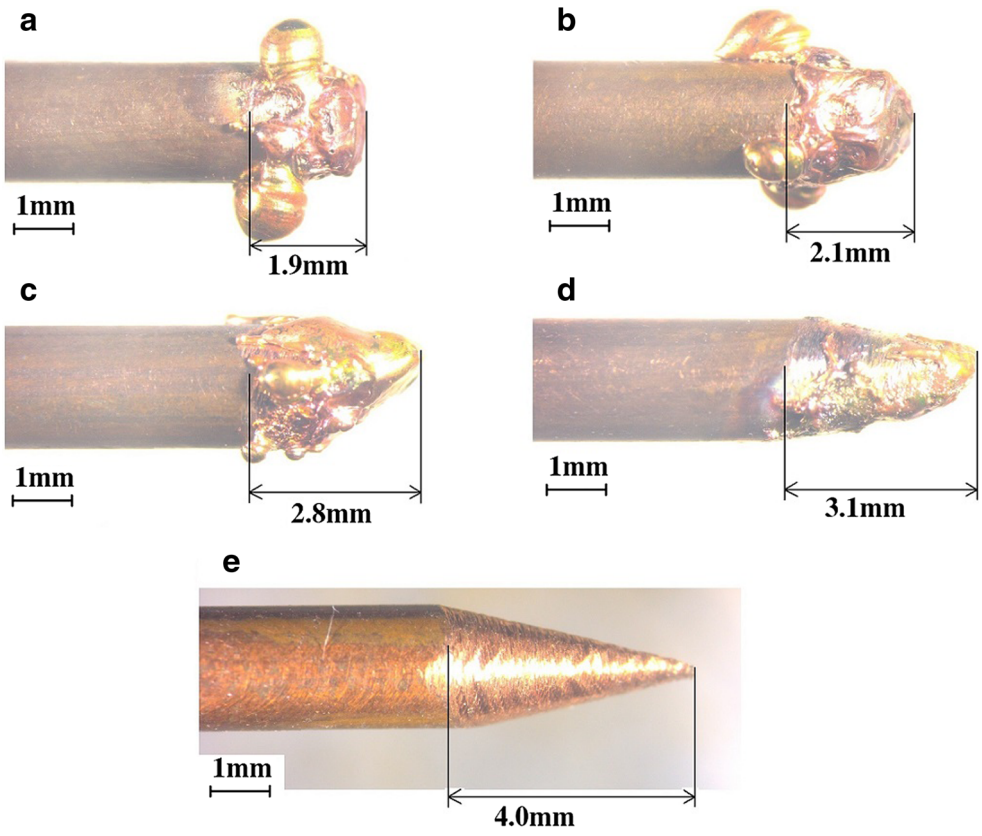

Fig. 9 Needle electrode wear erosion shape: **a** no flushing, **b** 15 m/s, **c** 30 m/s, **d** 45 m/s, **e** initial shape

was quite diverse under different air flushing velocities, and the wear length of the electrode decreased as the air flushing velocity increased. As shown in Fig 9a and b, the tip of the electrode was almost eroded completely after discharge. As the air flushing velocity increased, the erosion area mainly focused on the back of the electrode, as shown in Fig. 9c–d. The most possible reason is that the flushing air drives the arc plasma heat source to the back of electrode, which can be observed in Fig. 6. Additionally, it is notable that higher air flushing velocity can cool down the arc discharge zone more effectively and result in less tool wear.

6 Conclusion

In this research, the mechanism of arc plasma channel expansion and deflection under air flushing was studied. Additionally, the influence of air flushing velocity on arc plasma movement was analyzed. Based on the observed experimental and theoretical analysis, the following conclusions can be drawn:

(1) In air-based arc discharging, arc plasma initially expands and then moves. In each pulse duration, the arc plasma column experiences three stages: rapid radial expansion, full expansion, and deflection. In the radial expansion stage, the arc plasma increases its diameter while maintaining its length, and its average radial expansion speed can reach up to $20m/s$. In the full-expansion stage, both the diameter and length of the arc plasma increase with a limited speed, measuring approximately 1.8 m/s and 0.87 m/s, respectively. In the plasma excursion stage, the average movement velocity of the arc plasma is 1.85 m/s.

(2) The interaction between arc plasma self-magnetic compression and air flushing effect was studied. The additional increment in pressure of plasma arc column was introduced to analyze the reason for arc plasma deflection in different stages. The deduced equation indicated that the value of the additional increment in pressure was related to radius of plasma arc column.

(3) The degree of arc plasma deflection increases with the increasing air flushing velocities. When the velocity is high, the front interface is compressed and the back interface is enlarged and excursed together with a fluctuating current and voltage waveforms, which discloses that the arc plasma is disturbed effectively. As the flushing velocity increases to 45 m/s, the plasma column is elongated to a near broken status, which proves the feasibility of hydrodynamic arc breaking mechanism in air-based blasting erosion arc machining.

(4) When discharging in high-velocity air flushing, a trailing discharge crater with eliminated recast molten metal is obtained on the workpiece surface, which indicates that the air flushing can effectively expel the melted metal from the molten pool. It is also noted that the electrode wear length decreases significantly as the air flushing velocity increases, which indicates that air flushing can help to decrease the tool wear.

Funding information The authors received financial support from the National Science Foundation of China (Grant No. 51235007, 51575351) and the State key Laboratory of Mechanical System and Vibration of China (Grant No. MSV201305) .

References

1. Xu H, Gu L, Chen J, Hu J, Zhao W (2015) Machining characteristics of nickel-based alloy with positive polarity blasting erosion arc machining. Int J Adv Manuf Technol 79(5-8):937–947
2. Chen J, Gu L, Xu H, Zhao W (2016) Study on blasting erosion arc machining of ti"C6al"C4v alloy. Int J Adv Manuf Technol 85(9-12):2819–2829
3. Gu L, Chen J, Xu H, Zhao W (2016) Blasting erosion arc machining of 20 vol.% sic/al metal matrix composites. Int J Adv Manuf Technol 87(9-12):2775–2784
4. Zhao W, Gu L, Xu H, Li L, Xiang X (2013) A novel high efficiency electrical erosion process "C blasting erosion arc machining ¡î. Procedia Cirp 6(6):621–625
5. Gu L, Zhang F, Zhao W, Rajurkar KP, Malshe AP (2016) Investigation of hydrodynamic arc breaking mechanism in blasting erosion arc machining. CIRP Ann Manuf Technol 65(1):233–236
6. Zhang F, Gu L, Chen J, Xu H, Zhao W (2015) Observation and modeling research of high-velocity flushing effect on the performance of beam. Int J Adv Manuf Technol 86(1-4):1–8
7. Kunieda M, Yoshida M, Taniguchi N (1997) Electrical discharge machining in gas. CIRP Ann Manuf Technol 46(1):143–146
8. Kunleda M, Miyoshi Y, Takaya T, Nakajima N, Yu ZB, Yoshida M (2003) High speed 3d milling by dry edm. CIRP Ann Manuf Technol 52(1):147–150
9. Kunieda M, Takaya T, Nakano S (2011) Improvement of dry edm characteristics using piezoelectric actuator. CIRP Ann Manuf Technol 53(1):183–186
10. Zhang M, Zhang Q, Wang H, Liu G, Guo T (2015) Research on a single pulse discharge to discriminate edm and eam based on the plasma tunnel and crater geometry. J Mater Process Technol 219:248–256
11. Shen Y, Liu Y, Sun W, Dong H, Zhang Y, Wang X et al (2015) High-speed dry compound machining of ti6al4v. J Mater Process Tech 224:200–207
12. Maecker HH (1971) Principles of arc motion and displacement. Proc IEEE 59(4):439–449
13. Kojima A, Kunieda M (2007) Study of thermal equilibrium of edm arc plasma by spectroscopy. Journal of the Japan Society of Electrical Machining Engineers 41(97):56–60
14. Zhu Y, Farhadi A, He G, Liu X, Gu L, Zhao W (2018) Influence of gap air flushing on plasma channel and crater geometry in single blasting erosion arc discharge ¡î. Procedia Cirp 68:210–214

15. Farhadi A, Zhu Y, Gu L, Zhao W (2018) Influence of electrode shape and size on electric arc channel and crater ¡î. Procedia Cirp 68:215–220
16. Natsu W, Ojima S, Kobayashi T, Kunieda M (2004) Temperature distribution measurement in edm arc plasma using spectroscopy. JSME Int J 47(1):384–390
17. Kitamura T, Kunieda M, Abe K (2015) Observation of relationship between bubbles and discharge locations in EDM using transparent electrodes. Precis Eng 40:26–32
18. M.Steenbeck Z (1932) Phys. 33:809
19. Pan J, Hu S, Yang L, Chen S (2016) Numerical analysis of the heat transfer and material flow during keyhole plasma arc welding using a fully coupled tungsten“Cplasma”Canode model. Acta Mater 118:221–229
20. Ogino Y, Hirata Y, Kawata J, Nomura K (2013) Numerical analysis of arc plasma and weld pool formation by a tandem tig arc. Welding in the World 57(3):411–423